Journal of Non-Crystalline Solids 356 (2010) 1252–1257

Glass formation from iron-rich phosphate melts

L. Zhang [a], R.K. Brow [a,*], M.E. Schlesinger [a], L. Ghussn [b], E.D. Zanotto [b]

[a] Department of Materials Science and Engineering, Missouri University of Science and Technology, 1400 N. Bishop Avenue, Rolla, MO 65409-0340, USA
[b] Universidade Federal de São Carlos, Vitreous Materials Laboratory, LaMaV, Rod. Washington Luis, Km. 235, 13.565-905 São Carlos, Brazil

ARTICLE INFO

Article history:
Received 18 August 2009
Received in revised form 14 April 2010
Available online 17 May 2010

Keywords:
Iron phosphate glasses;
Iron-rich phosphate;
Glass formation;
Glass structure

ABSTRACT

Iron-rich phosphate glasses with nominal Fe/P ratios between 1.0 and 1.6 were prepared by a roller-quenching technique. The critical cooling rates (CCR) for glass formation were estimated by differential thermal analysis and found to be in the range of 10^3–10^4 °C/s for the iron-rich melts, compared to 1–10 °C/s for conventional iron phosphate melts with nominal Fe/P ratios near 0.50. The Fe(II)/Fe_{total} fraction in the quenched glasses increases with melt time and temperature, and ranges between 0.30 and 0.55 for the glasses studied. Raman spectroscopy indicates that the structures of the iron-rich phosphate glasses are based on isolated orthophosphate tetrahedra, similar to what are found in α-$FePO_4$.

1. Introduction

Iron phosphate glasses have been developed as alternative materials for high-level nuclear waste encapsulation [1–8]. The glasses can dissolve large quantities of a variety of waste components while retaining outstanding chemical durability. Iron phosphate glasses also exhibit interesting electrical and magnetic properties that depend on the iron coordination number and redox state [9,10].

Iron phosphate compositions with nominal Fe/P atom ratios between 0.33 and 0.67 have good glass forming ability (GFA) and have been widely studied [1–8]. Phosphate-rich ferrous ultraphosphate glasses ($FeO/P_2O_5 < 1:1$) were made in sealed silica tubes under vacuum and their structures and properties characterized [11,12]. Glasses with Fe/P ratios as high as 1.83 have been prepared by quenching microwave- or joule-heated melts between pre-cooled copper plates [13], but the structure and properties of these iron-rich glasses were not investigated. Glasses with Fe/P ratios between 1.0 and 2.3 were made by twin-roller-quenching [14], and the magnetic properties of one glass (Fe/P = 2.3) were reported. However, little is known about the structure and thermal stability of iron-rich (Fe/P > 1) phosphate glasses.

The structures of iron phosphate glasses with Fe/P ratios between 0.33 and 0.67 are reported to be similar to the short range structure of crystalline $Fe_3(P_2O_7)_2$ [7]. Ferrous and ferric ions in distorted octahedral sites are assumed to link neighboring pyrophosphate anions to constitute the glass structure. The fraction of ferrous ions, Fe^{2+}/Fe_{total}, in the quenched glasses increases with melting temperature and with iron content. For conventional iron phosphate glasses, Fe^{2+}/Fe_{total} is below 0.4 and melts with $Fe^{2+}/Fe_{total} \geq 0.4$ crystallize more rapidly when quenched in air by pouring into steel molds [7].

It is well-known that GFA is enhanced for melt compositions near deep eutectics [15–17]. GFA can be characterized using critical cooling rate (CCR) experiments to determine the conditions required to avoid crystallization upon quenching. Turnbull proposed that GFA was related to the ratio between the glass transition temperature (T_g) and the liquidus temperature (T_L); the greater T_g/T_L, the better the GFA [18]. Other common glass stability (GS) parameters are listed in Table 1. These GS parameters were evaluated by Nascimento, et al. [23] using thermal analytical information and related to GFA for eight different glass forming systems. The three GS parameters listed in Table 1 correlate well with experimental measurements of GFA, and their respective critical cooling rate relationships are also given in Table 1.

The liquidus surface of the Fe_3PO_7–$FePO_4$ system was reported by Wentrup [24] to have a eutectic point at Fe/P = 1.38 (molar). This system has been re-investigated as part of a larger study of the Fe_2O_3–P_2O_5 liquidus surface that is to be published elsewhere [25]; a similar eutectic composition was found, but at a greater eutectic temperature (1070 °C vs. 968 °C) than reported by Wentrup.

In the present study, the glass forming tendencies of iron phosphate melts with initial molar compositions around the reported eutectic point of the Fe_3PO_7–$FePO_4$ system ($1.00 \geq Fe/P \geq 1.60$) were investigated. The melts studied here have significantly greater iron contents than typical iron phosphate glasses, and Raman spectroscopy indicates that these glasses possess "invert" structures [26] based on isolated orthophosphate tetrahedra linked through iron polyhedra. The glass forming ability of these melts was studied using DTA characterization and the GS parameters in Table 1.

* Corresponding author. Tel.: +1 573 341 6812; fax: +1 573 341 2071.
E-mail address: Brow@mst.edu (R.K. Brow).

0022-3093/$ – see front matter © 2010 Elsevier B.V. All rights reserved.
doi:10.1016/j.jnoncrysol.2010.04.019

Table 1
GS parameters and calculation equation.

GS parameter	Reference	Equation for critical cooling rate (°C/s), from ref. [23]
$K_T = \frac{T_g}{T_L}$	[18]	–
$K_L = \frac{T_X^p}{T_g + T_L}$	[19,20]	CCR = 16.7–33.1 K_L
$K_W = \frac{T_X^p - T_g}{T_L}$	[21]	CCR = 4.0–20.5 K_W
$K_H = \frac{T_X^p - T_g}{T_L - T_X^p}$	[22]	CCR = 3.0–2.44 K_H

T_g is the glass transition temperature, T_L is the melt liquidus temperature, and T_X^p is the peak temperature for crystallization. All temperatures are in Kelvin.

2. Experimental procedures

Compositions near the eutectic point between $FePO_4$ and Fe_3PO_7, with nominal Fe/P atom ratios between 1.0 and 1.6, were investigated, along with compositions of conventional iron phosphate glass (Fe/P = 0.5, 0.67 and 0.82). Mixtures of reagent grade Fe_2O_3 (Alfa Aesar, ≤45 μm, ≥99%) and $FePO_4$, obtained by dehydrating $FePO_4 \cdot xH_2O$ (>99%, Alfa Aesar), weighing 2-5 grams were used to prepare the iron-rich (Fe/P ≥ 1.0) phosphate glasses. Mixtures of $NH_4H_2PO_4$ (Alfa Aesar, 98%) and Fe_2O_3 were used to prepare 10–30 g of the conventional (Fe/P < 1.0) iron phosphate glasses. For all glasses, the raw materials were thoroughly mixed and then heated in alumina crucibles for the times and temperatures indicated in Table 2. Melts were quenched either by cooling thick (2–4 mm) patties in air, by pressing thin (~1 mm) samples between steel plates, or by preparing very thin (<100 μm) ribbons with a twin-roller quencher. The distance between the two rollers and the rotation rate could be adjusted to modify the ribbon thickness, and thus the quench rate.

The quenched samples were pulverized to <53 μm and analyzed by X-ray diffraction (XRD Scintag XDS 2000) and differential thermal analysis (Perkin-Elmer DTA7). The DTA runs were performed in air at a heating rate of 10 °C/min. Characteristic temperatures from the DTA experiments were used to calculate CCRs based on the equations reported by Nascimento, et al. [23] and summarized in Table 1.

The melting times and temperatures were varied for some samples to study processing effects on the FE^{2+}/Fe_{total} ratio. The Fe^{2+}/Fe_{total} ratios in the glasses were determined by a titration method [27] with 2 mM $KMnO_4$. Raman spectra (Horiba-Jobin Yvon LabRam-HR) in the range of 50–2000 cm^{-1} were collected using a He–Ne laser (632.8 nm) on glass powders and on powders of crystalline α-$FePO_4$ and $Fe_3(P_2O_7)_2$. Powders from roller-quenched iron-rich (Fe/P ≥ 1) glasses were analyzed, along with powders from plate-quenched conventional (Fe/P < 1) glasses. α-$FePO_4$ was prepared by dehydrating $FePO_4 \cdot xH_2O$ at 880 °C for ~24 h. $Fe_3(P_2O_7)_2$ was prepared by heating stoichiometric mixtures of $Fe_4(P_2O_7)_3$ and $Fe_2P_2O_7$ in sealed silica tubes for 12 h at 900 °C. $Fe_4(P_2O_7)_3$ was initially prepared using methods reported in [28], and $Fe_2P_2O_7$ was prepared by reducing $FePO_4$ in forming gas (10% H_2 and 90% Ar) at 560 °C.

Table 2
Glass compositions and the melting conditions.

Initial Fe/P ratio	Melting temperature (°C)	Melting time (h)
1.60	1250	2
1.50	1200	2
1.38	1150	0.5, 1.0, 2.0, 6.0
1.38	1200	0.5, 2
1.30	1200	2
1.00	1250	2
1.00	1300	0.5, 1.0, 2.0, 6.0
0.82	1200	2
0.67	1200	2
0.50	1200	2

3. Results

3.1. Glass forming tendency

Fig. 1 shows the XRD patterns of glasses from (a) a roller-quenched Fe/P = 1.30 melt and (b) the same melt after quenching between steel plates. The broad diffuse peak in the pattern for the roller-quenched glass indicates the amorphous state of the sample. The crystalline phases detected in this partially crystallized, plate-quenched sample are $FePO_4$, $Fe_3(P_2O_7)_2$ and $Fe_7(PO_4)_6$.

Table 3 summarizes the XRD analyses of glasses prepared from melts with different nominal compositions and quenched by different means. Every sample prepared from the iron-rich melts (Fe/P ≥ 1.0) exhibited evidence of crystallization when cooled in air or between steel plates. However, the roller-quenched melts yielded glasses with no detectable crystallinity. The cooling rates that each method can achieve depend on the melt temperature, sample size and other experimental conditions. From reports in the literature, cooling in air from temperatures below 1300 °C and pressing from 1300 °C between steel plates can achieve cooling rates in the range of $10–10^3$ °C/s [23,29]. Twin-roller-quenching can achieve cooling rates as high as 10^6 °C/s [30].

3.2. The dependence of Fe(II) content on melt conditions

Fig. 2 shows that the relative Fe(II) content of roller-quenched, iron-rich glasses increases with melt time, reaching a constant value after about 1 h. Fig. 3 shows that the Fe(II) content increases with melt temperature, and that glasses with greater Fe/P ratios have greater Fe (II) contents when quenched from melts held at the same temperature. A model to predict the effects of melt composition, atmosphere and temperature on the equilibrium Fe^{2+}/Fe_{total} ratio has been developed and will be reported elsewhere [31].

3.3. Thermal characteristics

Fig. 4 shows DTA patterns collected in air for several glasses (melting time: 2 h) investigated in this work. In general, for glasses melted under similar conditions, T_g increases and the peak temperature for crystallization (T_X^p) decreases with increasing Fe/P ratio, as summarized in Fig. 5. (Note that the characteristic temperatures for the iron-rich glasses were obtained from roller-quenched samples, whereas plate-quenched samples of the conventional iron phosphate glasses were evaluated.) The estimated uncertainty of these

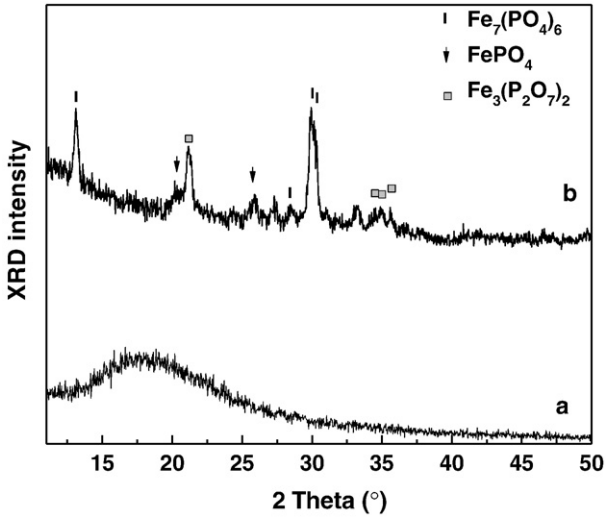

Fig. 1. XRD patterns from samples quenched from melts with a nominal Fe/P = 1.30, held for 2 h at 1200 °C, then a) roller-quenched, or b) quenched between steel plates.

Table 3
Major crystalline phases detected by XRD from Fe_2O_3–P_2O_5 melts quenched by different methods; all melting time was 2 h.

Nominal (Fe/P ratio)	Air quench	Steel quench	Roller quench
0.50	None detected	None detected	None detected
0.67	None detected	None detected	None detected
0.82	$FePO_4$, $Fe_3(P_2O_7)_2$	None detected	None detected
1.00	$FePO_4$, $Fe_2P_2O_7$	$FePO_4$, $Fe_2P_2O_7$	None detected
1.30	$Fe_7(PO_4)_6$, $Fe_3(P_2O_7)_2$, $FePO_4$	$Fe_7(PO_4)_6$, $Fe_3(P_2O_7)_2$, $FePO_4$	None detected
1.38	$FePO_4$, $Fe_3(P_2O_7)_2$	$FePO_4$, $Fe_3(P_2O_7)_2$	None detected
1.50	$FePO_4$, $Fe_7(PO_4)_6$	$FePO_4$, $Fe_7(PO_4)_6$	None detected
1.60	$FePO_4$, $Fe_7(PO_4)_6$, Fe_3PO_7	$FePO_4$, $Fe_7(PO_4)_6$, Fe_3PO_7	None detected

temperatures is ±5 °C based on the multiple DTA runs. Also shown in Fig. 5 are the liquidus temperatures (T_L) for the respective melts, as reported elsewhere [25]. The values of ($T_X^p - T_g$) for the iron-rich (Fe/P ≥ 1.0) glasses are much smaller (35–67 °C) than that (~300 °C) of the conventional iron phosphate glass (Fe/P = 0.50). This is consistent with the much better glass forming tendency of the latter composition, as indicated by the XRD results summarized in Table 3. Mogušić-Milanković, et al. [32] report a similar decrease in ($T_X^p - T_g$) with increasing Fe/P content for a much smaller range of iron phosphate glass compositions.

3.4. Glass structure

Raman spectra collected from plate-quenched glasses with nominal Fe/P ratios less than 1.0 are compared with that collected from crystalline $Fe_3(P_2O_7)_2$ in Fig. 6. For $Fe_3(P_2O_7)_2$, peaks in the range of 1000–1200 cm^{-1} can be assigned to symmetric and asymmetric stretching modes of P–O bonds in the pyrophosphate anions [33]. The low intensity peak near 760 cm^{-1} is assigned to a P–O–P stretching mode, the peak near 670 cm^{-1} is assigned to a P–O bending mode, and the series of peaks below 400 cm^{-1} are assigned to various Fe–O and P–O modes. The Raman spectra from the iron phosphate glasses have a broad peak centered near 1030–1050 cm^{-1}, several low intensity peaks below 600 cm^{-1}, and, for the glasses with Fe/P = 0.50 and 0.67, a less intense peak between 690 and 800 cm^{-1}. The broad peak centered near 1030–1050 cm^{-1} has been assigned to the symmetric and asymmetric stretching modes of non-bridging oxygens associated with different phosphate tetrahedra; for example, non-bridging oxygens on tetrahedra with one bridging oxygen (Q^1 tetrahedra) account for peaks near 1030–1050 cm^{-1} and those on tetrahedra with two bridging oxygens (Q^2) account for shoulders near 1200 cm^{-1} [34,35]. The peak between 600 and 800 cm^{-1} is assigned to the symmetric stretching mode of bridging oxygens, $(P–O–P)_{sym}$, in the glass structure [36]. The similarity in the spectra from these glasses with that from crystalline $Fe_4(P_2O_7)_2$ is consistent with the proposal that these glasses possess short range structures that are similar to the short range structure of crystalline $Fe_4(P_2O_7)_2$ [7]. In particular, these glasses possess pyrophosphate anions that are linked by ferrous and ferric polyhedra.

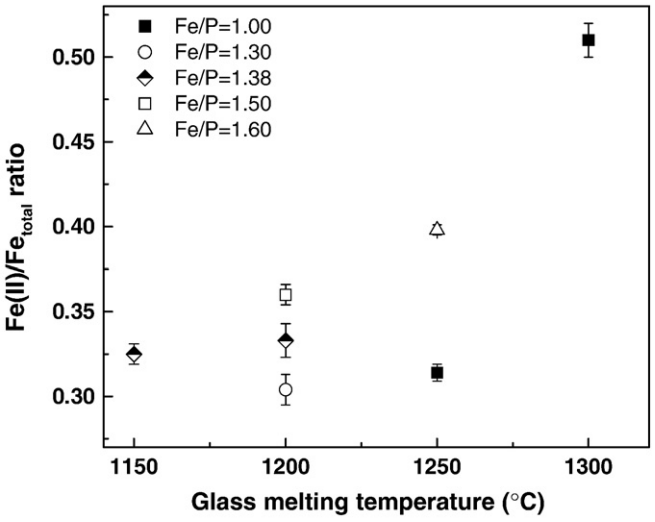

Fig. 3. Summary of the Fe(II)/Fe_{total} ratios of roller-quenched glasses from melts held for 2 h at different temperatures.

Raman spectra collected from roller-quenched iron-rich glasses (Fe/P ≥ 1.00) are shown in Fig. 7, and are compared with that collected from crystalline α-$FePO_4$. The Raman spectra from the iron-rich glasses are distinctly different from those of the conventional iron phosphate glasses, shown in Fig. 6. The spectra from the iron-rich glasses are dominated by an intense peak centered near 1002 cm^{-1}, as well as a number of lower intensity peaks in the range between 100 and 500 cm^{-1}. The peak centered near 1002 cm^{-1} is assigned to $P–O^-$ stretching modes of non-bridging oxygens on Q^0 tetrahedra, consistent with the spectrum from α-$FePO_4$, where this peak is found at 1009 cm^{-1}. This peak is broader (full width at half-maximum = 30–50 cm^{-1}) in the spectra from the glasses than that

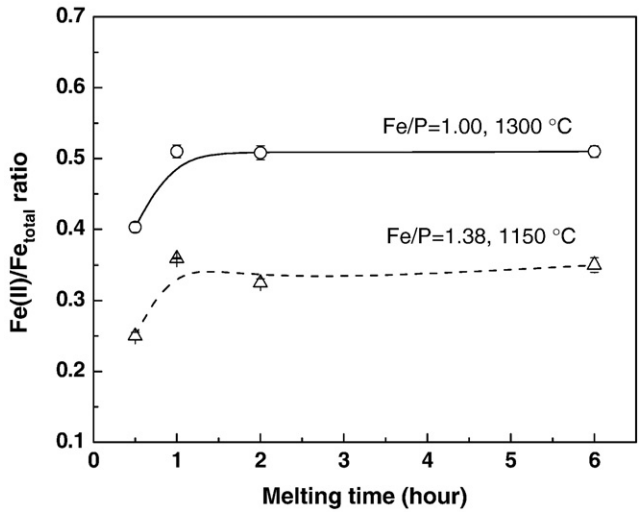

Fig. 2. Fe(II)/Fe_{total} ratios for two sets of roller-quenched glasses prepared from melts held at different temperatures for up to 6 h. Lines are added as guides for the eye.

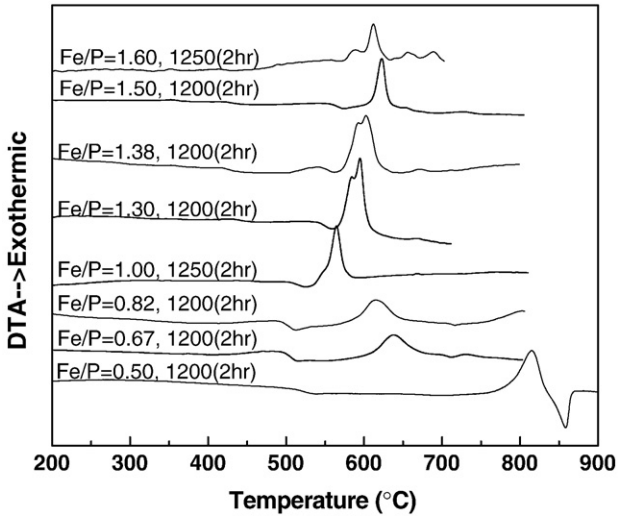

Fig. 4. DTA patterns of iron-rich phosphate glasses; the data were collected in air at 10 °C/min.

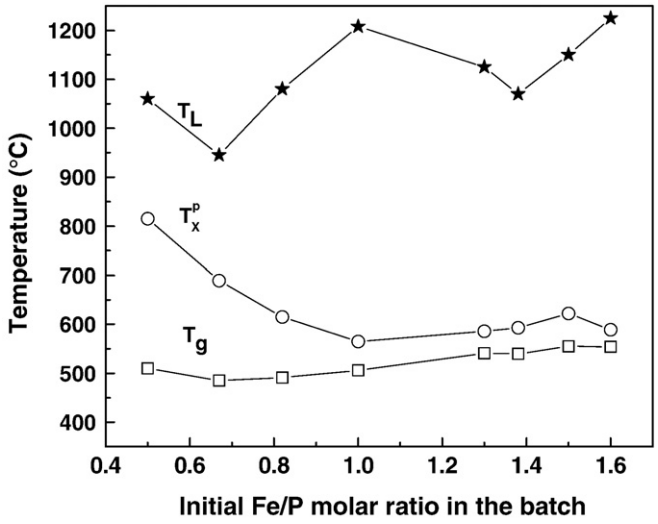

Fig. 5. Characteristic temperatures of the glasses investigated in this work, determined by DTA. Liquidus temperatures are from ref. [25]. Lines are added as guides for the eye.

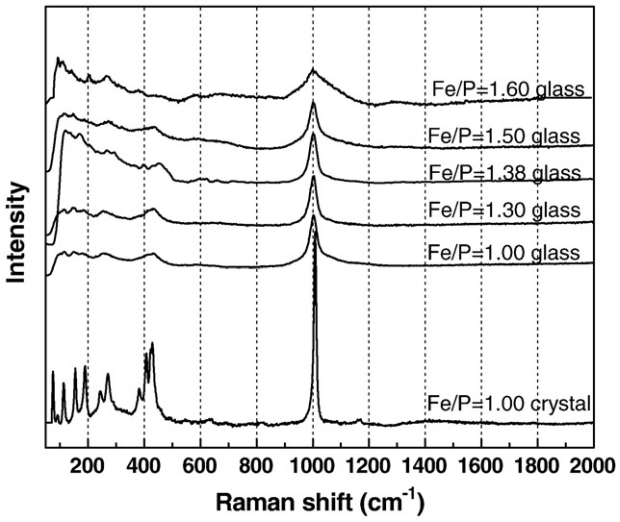

Fig. 7. Raman spectra of iron-rich glasses compared to crystalline $FePO_4$.

obtained from α-$FePO_4$ (FWHM = 10 cm^{-1}), consistent with a greater degree of disorder associated with these roller-quenched glasses. (The glass with Fe/P = 1.6 fluoresced substantially when the Raman spectra were collected. This might contribute to the relative broadening of the 1000 cm^{-1} peak noted for this sample in Fig. 7.) The broadening and decrease in frequency of this peak for the glasses, compared to α-$FePO_4$, is consistent with what was reported by Burba, et al. [37] in their recent study of crystalline and disordered α-$FePO_4$. There is no distinct evidence for non-bridging oxygen modes at greater wave numbers in the Raman spectra of the iron-rich glasses, nor for the $(P–O–P)_{sym}$ stretching mode near 700 cm^{-1}. The peaks between 400 and 500 cm^{-1} arise from the O–P–O bending modes of Q^0 units [32,38]. The peaks at ~260 cm^{-1} are likely related to the bending Q^0 with Fe as modifier [38]. The peaks below 200 cm^{-1} have been assigned to both P–O and Fe–O modes [39,40]. The similarity in the spectra from the iron-rich glasses with the spectrum from α-$FePO_4$ in Fig. 7 indicates that similar P- and Fe-tetrahedra likely exist in the glasses.

4. Discussion

4.1. Glass formation and structure

Fig. 8 compares the glass forming range (region "a") for conventional iron phosphate glasses based on the reported data [6,7,9], with the glass forming range for the new iron-rich phosphate glasses studied in this work (region "b"). Here, the open symbols represent the compositions of the glass batches and the "x" symbols within region "b" indicate the compositions of the iron-rich, X-ray amorphous glasses prepared by roller-quenching. The reduction of Fe^{3+} to Fe^{2+} during melting decreases the O/P ratios of these quenched glasses from their nominal values. The heavy line in Fig. 8 indicates compositions with an O/P ratio of 4.0; compositions below this line have O/P>4.0. The new glass forming range (region "b") for iron-rich compositions is bounded by the crystalline phases $FePO_4$, $Fe_2P_2O_7$, $Fe_3(P_2O_7)_2$, Fe_3PO_7 and $Fe_7(PO_4)_6$, each of which has been identified by XRD in various partially crystallized samples (Table 3).

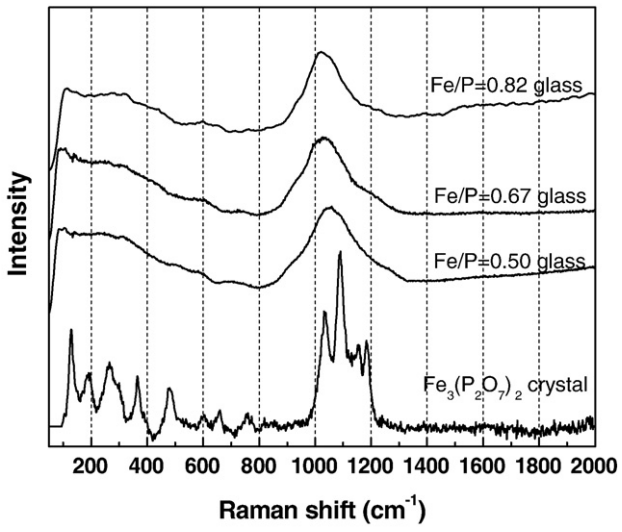

Fig. 6. Raman spectra of the glasses with Fe/P ≤ 1.00 compared to crystalline $Fe_3(P_2O_7)_2$.

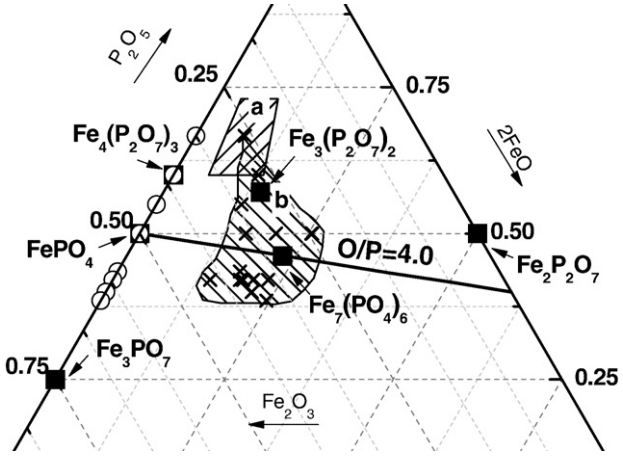

Fig. 8. Compositions of iron-rich glasses prepared in this study. ○ — nominal composition of the batch; × — analyzed glass composition after roller-quenching (Table 2); ■ — crystalline phases identified in partially crystallized samples (Table 3). Region "a" is the glass forming region for typical iron phosphate glasses [6,7] and region "b" includes the iron-rich compositions identified in the present study.

It is worth emphasizing that the reported glass forming range for the conventional iron phosphate glasses (region "a" in Fig. 8) represent lower quenching rates (as cast or plate quench) than are obtained by the roller quench techniques used to produce the iron-rich glasses (region "b"). It is expected that roller-quenching would increase substantially the glass forming range of meta- and polyphosphate compositions ($3 \leq O/P \leq 4$) beyond that indicated in "region a". In the present work, only roller-quenched melts near the orthophosphate ($O/P \geq 4$) composition were studied.

If the acidic phosphate units accept oxygens from the more basic iron oxide, then at $O/P = 4$, only non-bridging oxygens will be associated with the phosphate anions, forming isolated orthophosphate (Q^0) units that must be linked to neighboring iron polyhedra through the non-bridging oxygens. For glasses with $O/P > 4$, the additional oxygens must be incorporated into the structure in the form of Fe–O–Fe bonds, with little effect on the nature of the orthophosphate anions. (Similar "invert" structures have been reported for titanium-rich phosphate glasses [41].) The Raman spectra of the iron-rich glasses (Fig. 7) are dominated by a narrow peak at 1002 cm^{-1} that indicates the presence of the expected orthophosphate units, and this peak does not change with increasing Fe/P (and O/P) ratio. In contrast, the broad Raman peak centered near 1050 cm^{-1} in the spectrum of the Fe/P glass (Fig. 6) shifts to lower wavenumbers with increasing Fe/P ratio, consistent with the replacement of Q^2-tetrahedra by Q^1-tetrahedra as the overall O/P ratio increases. The Raman spectra indicate that the phosphate-rich compositions have larger phosphate anions that include Q^2 (middle units) and Q^1 (chain terminators) tetrahedra, whereas the iron-rich glasses possess only isolated (Q^0) tetrahedra. The relative complexity of the conventional glasses is reflected in the broader Raman peak associated with the P–O stretching modes (Fig. 6), compared to the respective peaks from the iron-rich glasses. A detailed description of the Raman spectra of iron phosphate compounds and glasses will be presented elsewhere. [42]

4.2. Critical cooling rate estimation

Fig. 9 shows the calculated critical cooling rates (CCRs) for the iron phosphate melts based on the characteristic temperatures shown in Fig. 5 and the equations listed in Table 1. The CCRs for the iron-rich ($Fe/P \geq 1.0$) phosphate melts are in the 10^3–10^4 °C/s range, compared to CCRs of 1–10 °C/s for conventional Fe–phosphate melts. The calculated CCRs indicate the difficulties of making iron-rich phosphate glass by quenching in air or pressing between metal plates. The tendency of CCR to increase with increasing Fe/P ratio is consistent with the glass forming experiments summarized in Table 3.

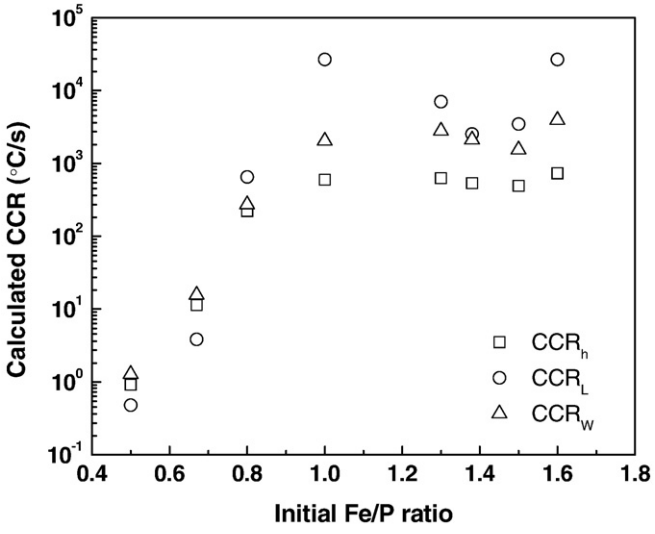

Fig. 9. Estimated CCRs for iron phosphate melts using characteristic temperatures from DTA experiments and the relationships in Table 1.

In general, phosphate glasses with longer phosphate chains (smaller O/P ratios) are more stable against devitrification. For example, Wange, et al. [43] report that crystallization tendency of a complex Ca-phosphate glass increases with increasing O/P ratio as smaller phosphate anions are available to constitute the glass structure. (Crystallization tendency also depends on the nature of oxides used to modify the glass; oxides that strengthen the glass network, like Al_2O_3 and TiO_2, increase viscosity and reduce crystallization tendency compared to oxides like CaO and Na_2O.) The addition of various oxides to an iron phosphate base glass tends to reduce the temperature difference between T_g and T_x, indicating an increase in crystallization tendency with increasing O/P ratio [8], although the extent of the temperature difference also depends on the nature of the oxide added. The enhanced crystallization behavior may be related to the changes in the rheological properties of phosphate glasses with shorter average phosphate chain-lengths. The rheological characteristics and the tendency of a phosphate melt to crystallize when sheared also depend on the type of phosphate anions that are present in the melt [44]. Smaller anions are often associated with faster crystallization.

The high CCR for glass formation from the iron-rich phosphate melts will limit the use of these glasses, particularly for applications like waste fixation that require the formation of relatively large samples with minimal crystallization. However, the expanded range of glass formation to the orthophosphate "invert" structures raises the likelihood that other compositions with similar structures can be developed, including those with a lower CCR. For example, the structures of the "NASICON" (sodium super-ionic conductors) family of glasses are based on orthophosphate ions and include ferric phosphate versions [45]. More recently, lithium-doped iron orthophosphate glasses have been produced in studies to develop cathode materials for Li-ion batteries [46]. The crystallization tendency of these glasses, determined by the difference in T_g and T_x obtained by DTA measurements, decreases with the addition of Li_2O.

5. Conclusion

Studies of glass formation and structure in the iron phosphate system have been extended to iron-rich compositions, with nominal Fe/P ratios in the range of 1.0–1.6. Critical cooling rates estimated from characteristic temperatures obtained by differential thermal analyses are at least 10^3 times greater for the new iron-rich compositions than for the conventional iron phosphate melts. The fraction of Fe(II) increases with increasing melt time and temperature. These new glasses have structures based on isolated phosphate tetrahedra (Q^0) and on Fe(II) and Fe(III) polyhedra.

Acknowledgements

The authors gratefully acknowledge Melodie L. Schmitt and Jong Wook Lim for their kind assistance and helpful discussion. This work is supported by the National Science Foundation (U.S.A.) under Grant DMR-0502463, CNPq (Brazil) Grant no. 492565/04-0 and FAPESP (Brazil) Grant 07/08179-9.

References

[1] B.C. Sales, L.A. Boatner, Science 226 (1984) 45.
[2] M.G. Mesko, D.E. Day, J. Nucl. Mater. 273 (1999) 27.
[3] S.T. Reis, M. Karabulut, D.E. Day, J. Nucl. Mater. 304 (2002) 87.
[4] W. Huang, C.W. Kim, C.S. Ray, D.E. Day, Ceram. Trans. 143 (2003) 347.
[5] W. Huang, D.E. Day, C.S. Ray, C.W. Kim, A. Mogus-Milankovic, J. Non-Cryst. Solids 327 (2004) 46.
[6] X. Fang, C.S. Ray, A. Mogus-Milankovic, D.E. Day, J. Non-Cryst. Solids 283 (2001) 162.

[7] G.K. Marasinghe, M. Karabulut, C.S. Ray, D.E. Day, M.G. Shumsky, W.B. Yelon, C.H. Booth, P.G. Allen, D.K. Shuh, J. Non-Cryst. Solids 222 (1997) 144.
[8] P.A. Bingham, R.J. Hand, O.M. Hannant, S.D. Forder, S.H. Kilcoyne, J. Non-Cryst. Solids 355 (2009) 1526.
[9] Y.M. Moustafa, K. El-Egili, H. Doweidar, I. Abbas, Phys. 353 (2004) 82.
[10] J.L. Shaw, A.C. Wright, R.N. Sinclair, G.K. Marasinghe, D. Holland, M.R. Lees, C.R. Scales, J. Non-Cryst. Solids 345&346 (2004) 245.
[11] U. Hoppe, M. Karabulut, E. Metwalli, R.K. Brow, P. Jovari, J. Phys Condens. Matter. 15 (2003) 6143.
[12] M. Karabulut, E. Metwalli, D.E. Day, R.K. Brow, J. Non-Cryst. Solids 328 (2003) 199.
[13] F.J.M. Almeida, J.R. Martinelli, C.S.M. Partiti, J. Non-Cryst. Solids 353 (2007) 4783.
[14] K. Tanaka, N. Soga, R. Ota, K. Hirao, Bull. Chem. Soc. Jpn 59 (1986) 1079.
[15] D.R. Uhlmann, J. Am. Ceram. Soc. 66 (1983) 95.
[16] W. Vogel, Glass Chemistry, 2nd ed.Springer, Berlin, 1985.
[17] H. Bürger, K. Kneipp, H. Hobert, W. Vogel, V. Kozhukharov, S. Neov, J. Non-Cryst. Solids 151 (1992) 134.
[18] D. Turnbull, Contemp. Phys. 10 (1969) 473–488.
[19] Z.P. Lu, C.T. Liu, Acta Mater. 50 (2002) 3501.
[20] Z.P. Lu, C.T. Liu, Phys. Rev. Lett. 91 (2003) 115505.
[21] M.C. Weinberg, Phys. Chem. Glasses 35 (1994) 119.
[22] A. Hruby, Czech J. Phys. B 22 (1972) 1187.
[23] M.L.F. Nascimento, L.A. Souza, E.B. Ferreira, E.D. Zanotto, J. Non-Cryst. Solids 351 (2005) 3296.
[24] H. Wentrup, Arch. Eisenhüt. 9 (1935) 57.
[25] L. Zhang, M. E. Schlesinger, R. K. Brow, "Phase Equilibria in the Fe2O3-P2O5 System" submitted to the Journal of the American Ceramic Society.
[26] H.J.L. Trapp, J.M. Stevels, Phys. Chem. Glasses 1 (1960) 107.
[27] S.I. Grishin, J.M. Bigham, O.H. Tuovinen, Appl. Environ. Microbiol. 54 (1988) 3101.
[28] L.K. Elbouaanai, B. Malaman, R. Gérardin, M. Ijjaali, J. Solid State Chem. 163 (2002) 412.
[29] M. Milanova, R. Iordanova, Y. Dimitriev, K. Kostov, S. Vassilev, J. Mater. Sci. 42 (2007) 3349.
[30] K.B.R. Varma, Bull. Mater. Sci. 9 (1987) 1.
[31] M. L. Schmitt, R. K. Brow, M. E. Schlesinger, "Predicting the Iron Redox Ratio in Iron Phosphate Melts: A Thermodynamic Model," submitted for publication.
[32] A. Moguš-Milanković, M. Rajić, A. Drašner, R. Trojko, D.E. Day, Phys. Chem. Glasses 39 (1998) 70.
[33] E.J. Baran, R.C. Mercader, A. Massaferro, E. Kremer, Spectrochim. Acta Part A 60 (2004) 1001.
[34] A. Mogus-Milankovic, B. Pivac, K. Furic, D.E. Day, Phys. Chem. Glasses 38 (1997) 74.
[35] C. Nelson, D.R. Tallant, Phys. Chem. Glasses 26 (1985) 119.
[36] A.M. Efimov, J. Non-Cryst. Solids 209 (1997) 209.
[37] C.M. Burba, J.M. Palmer, B.S. Holinsworth, J. Raman Spectrosc. 40 (2009) 225.
[38] A. Moguš-Milanković, A. Šantić, S.T. Reis, K. Furić, D.E. Day, J. Non-Cryst. Solids 342 (2004) 97.
[39] S. Okada, T. Yamamoto, Y. Okazaki, J. Yamaki, M. Tokunaga, T. Nishida, J. Power Sources 146 (2005) 570.
[40] C. Murli, S.M. Sharma, S.K. Kulshreshtha, S.K. Sikka, Pramana 49 (1997) 285.
[41] R.K. Brow, D.R. Tallant, W.L. Warren, A. McIntyre, D.E. Day, Phys. Chem. Glasses 38 (1997) 300.
[42] L. Zhang, R. K. Brow, M. E. Schlesinger, "Raman Spectra and the Structure of Iron Phospahte Compounds and Glasses," submitted for publication.
[43] P. Wange, J. Vogel, S. Knoche, C. Russel, Glass Sci. Technol. 77 (2004) 172.
[44] J.U. Otaigbe, G.H. Beall, Trends Polym. Sci. 5 (11) (1997) 369.
[45] T. Banu, K.K. Rao, M. Vithal, Phys. Chem. Glasses Eur. J. Glass Sci. Tech. B 44 (2003) 30.
[46] P. Jozwiak, J.E. Garbarczyk, M. Wasiucionek, I. Gorzkowska, F. Gendron, A. Mauger, C.M. Julien, Solid State Ionics 179 (2008) 46.